Supporting Information

Side–Reaction Modulation and Surface Reconfiguration of CoSe in Nitrate–to–Ammonia Reduction Reactions

Hao-Peng Lu [a, b], Xiao-Cheng Long [a, b], Ying-Ge Xu [c], Zu-Tao Pan [a, b], Lei Xian [a, b], Ling-Bin Kong [a, b]*

[a] State Key Laboratory of Advanced Processing and Recycling of Non-ferrous Metals, Lanzhou University of Technology, Lanzhou 730050, P. R. China

[b] School of Materials Science and Engineering, Lanzhou University of Technology, Lanzhou 730050, P. R. China

[c] Basic Subjects Department, Lanzhou Institute of Technology, Lanzhou 730050, People's Republic of China

* Corresponding author. E-mail: konglb@lut.edu.cn

Electrochemical characterization

In this work, the three–electrode system comprises a working electrode, a reference electrode, and a counter electrode. The reference electrode utilises a mercury/mercury oxide electrode, while the counter electrode is a platinum counter electrode. The working electrode consists of CC/NF that has undergone preliminary cleaning and been coated with the appropriate catalyst according to experimental requirements. The

platinum sheet is the counter electrode and the applied voltage is referenced to the Hg/HgO electrode (NaOH for the salt bridge solution) and the final potentials all require the use of the Nernst equation($E_{RHE}=E_{measured}+E^0_{Hg/HgO}+0.05916*Ph$， at 25 degrees Celsius$E^0_{Hg/HgO}$=0.1079 V) converted to a reversible hydrogen electrode potential (RHE). No iR compensation is applied to the test results in this work. Polarisation curves were obtained using linear voltammetric sweeping (LSV) at a sweep rate of 1 Mv s^{-1} over a fixed interval. Cyclic voltammetry tests (CV) were obtained in the non-Faraday interval (0-1.2 V vs. RHE) using sweep speeds of 20–100 mV s^{-1}. The electrochemically active area is proportional to the capacitance of the bilayer and is derived from the CV curve. Ammonia yield test was performed by stable catalysis of the working electrode in 80 mL of electrolyte for one hour for yield test.

The calculation of NO_3^-

The calculation formula was:

$$\text{NH}_3 \text{ yield（}\mu\text{g h}^{-1}\text{ mg}^{-1}\text{）} = \frac{c_{NH_3} \times V}{t \times m}$$

The Faraday efficiency is calculated as:

$$FE_{NH3}(\%) = \frac{n \times F \times c_{NH_3} \times V}{M \times Q} \times 100\%$$

Table S1：performance comparison

Materials	Ammonia yield	Faraday efficiency	Literatures
Cu NP	19.82	85.4	[1]
Co_3o_4	22.38	86.8	[2]
$Cu_3P@Co(OH)_2/CF$	3.23	86.7	[3]
Cu-CoO/NF	6.8	84	[4]
$La(OH)_3@CuCo$	8.8	76.6	[5]
$Ni_3Co_6S_8$	2.388	85.3	[6]
Fe HEA	3.25	92	[7]
$Cu/CoO_{0.65}Se_{VSe}$	2.36	93.5	[8]
$Co_{75}Me_{25}$	0.379	80.8	[9]
CoO/NF_{air}	15.66	76.08	This work
$CoSe/NF_{air}$	30.53	82.8	This work

Table S2：Elemental composition of CoSe prior to reaction by TEM EDS

Element	(keV)	Mass%	Counts	Sigma	Atom%	K
O K	0.525	1.95	3000.03	0.07	8.32	0.3849
Co K	6.924	22.73	31490.28	0.28	26.4	0.4284
Se L	1.379	75.32	44692.78	0.67	65.28	1

Table S3：Elemental composition of CoSe after to reaction by TEM EDS

Element	(keV)	Mass%	Counts	Sigma	Atom%	K
O K	0.525	18.23	8099.29	0.37	46.84	0.5042
Co K	6.924	59.8	13398.95	1.11	41.72	1
Se L	1.379	21.97	2108.6	0.92	11.44	2.3344

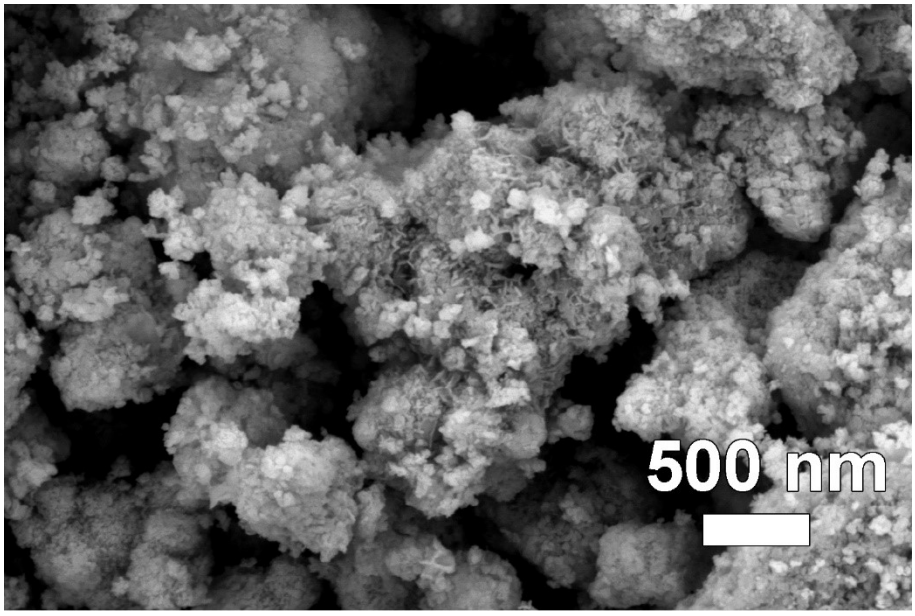

Fig. S1. The SEM spectra of CoSe.

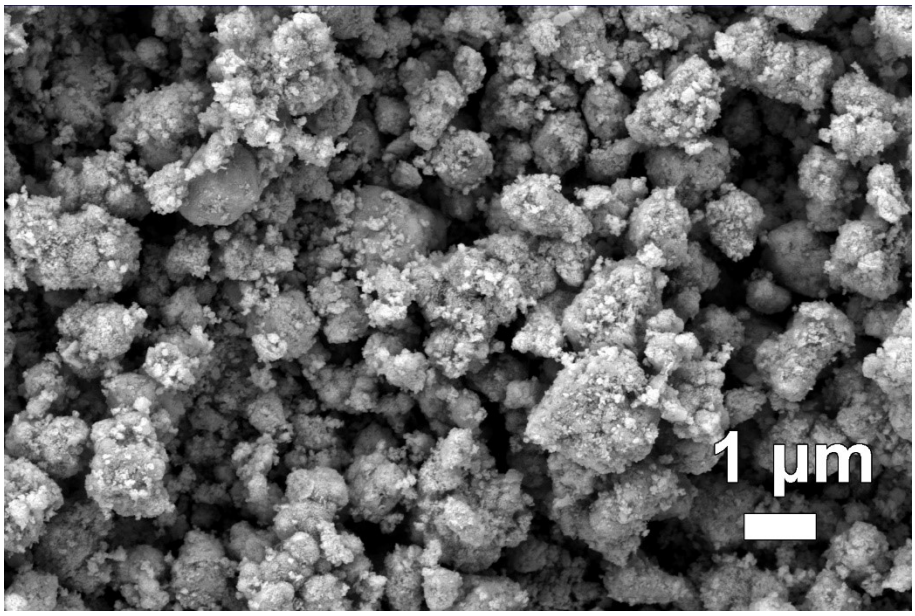

Fig. S2. The SEM spectra of CoSe.

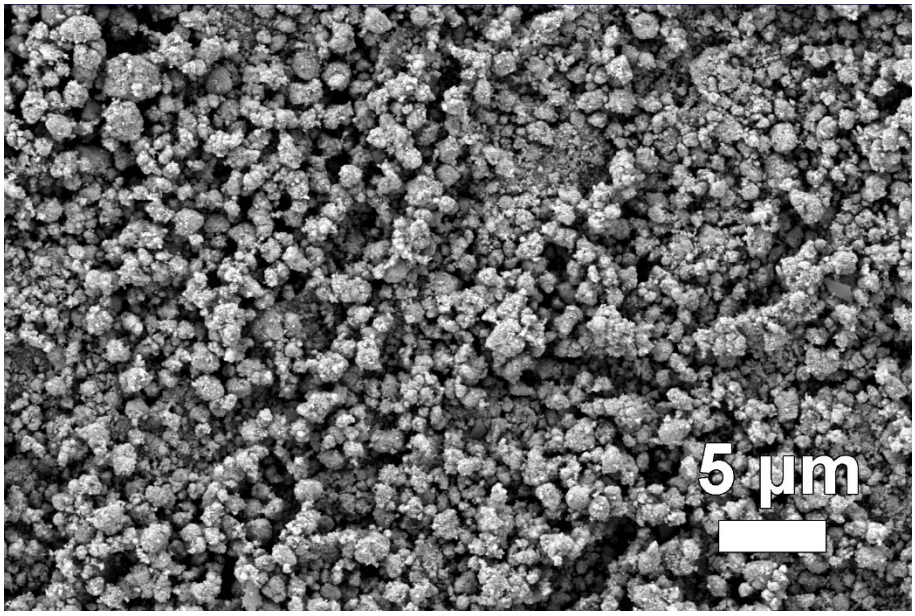

Fig. S3. The SEM spectra of CoSe.

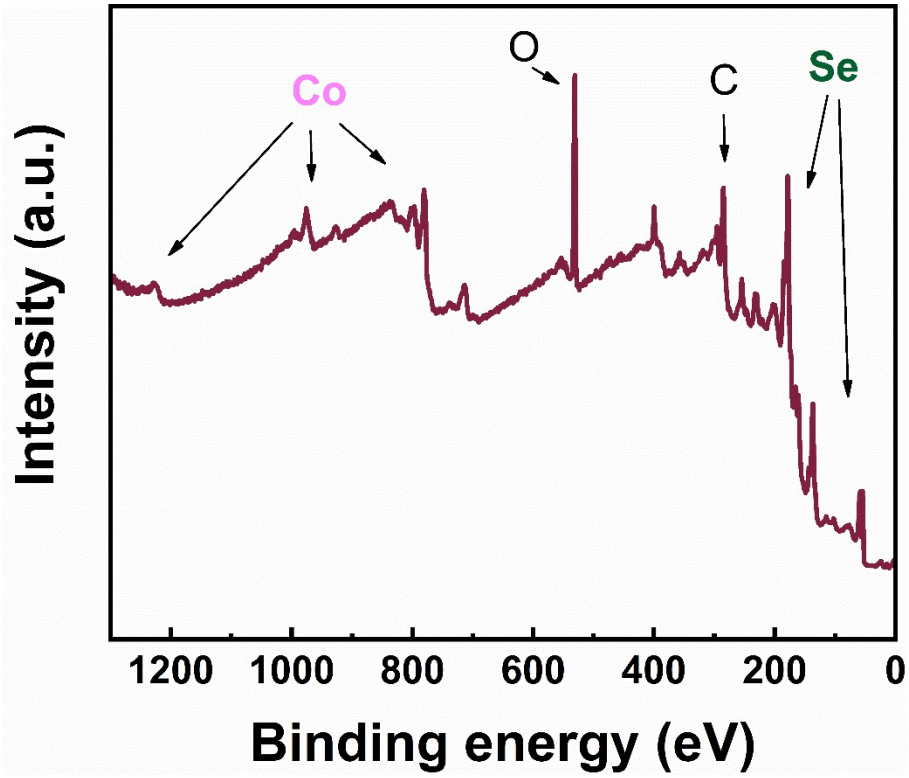

Fig. S4. The XPS full spectrum of CoSe.

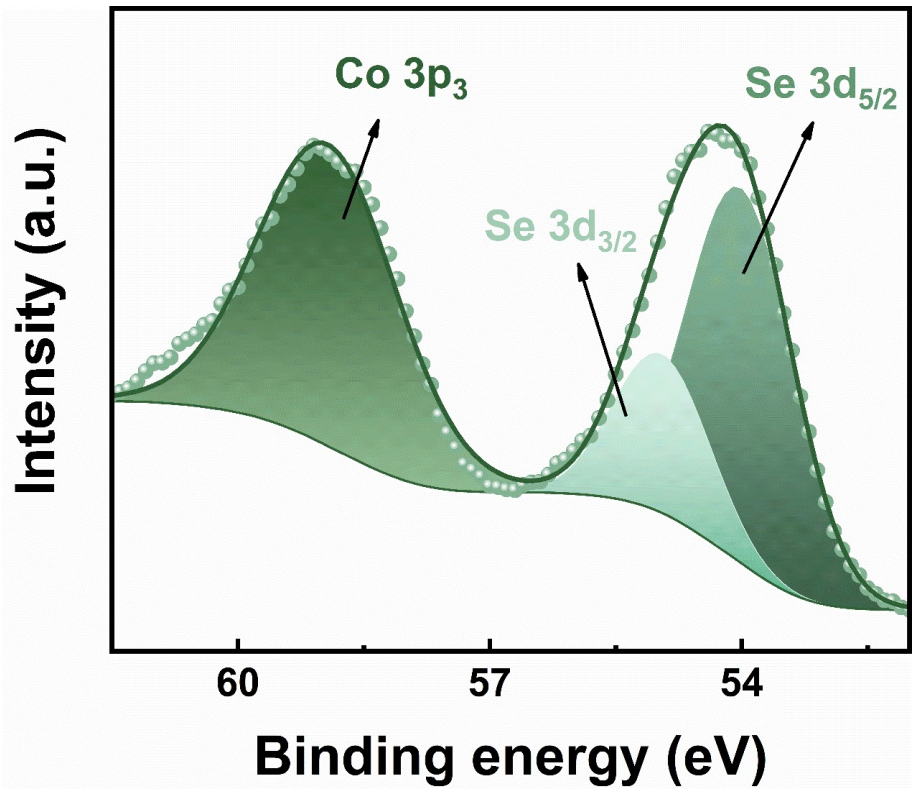

Fig. S5. XPS spectrum: elemental composition of selenium.

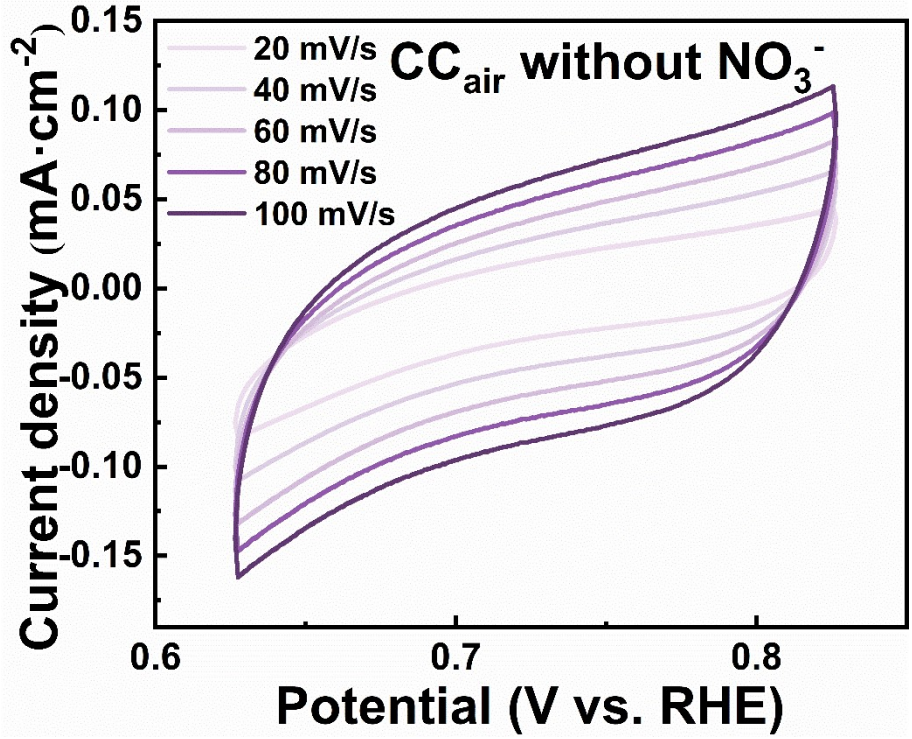

Fig. S6. The Plot of CV for CC in the absence of nitrate in the air environment.

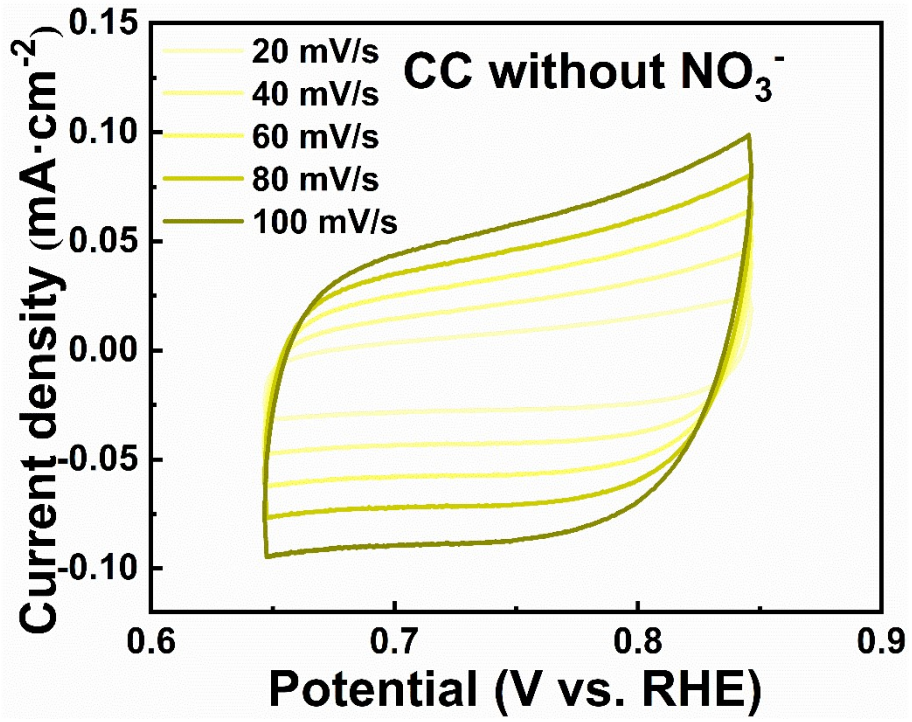

Fig. S7. The Plot of CV for CC without nitrate in an argon environment.

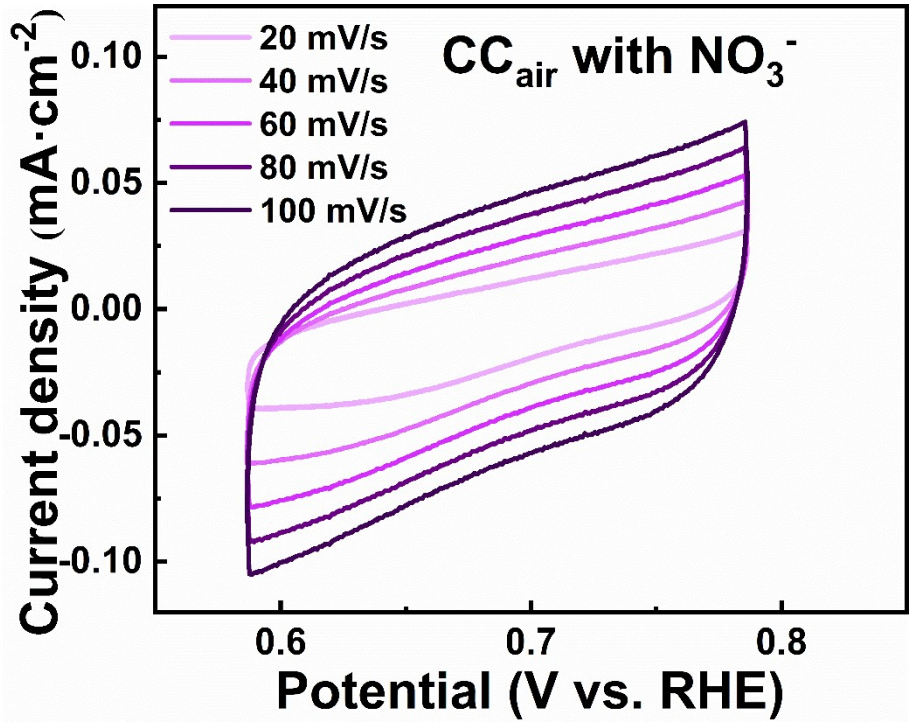

Fig. S8. The Plot of CV for CC with nitrate in the air environment.

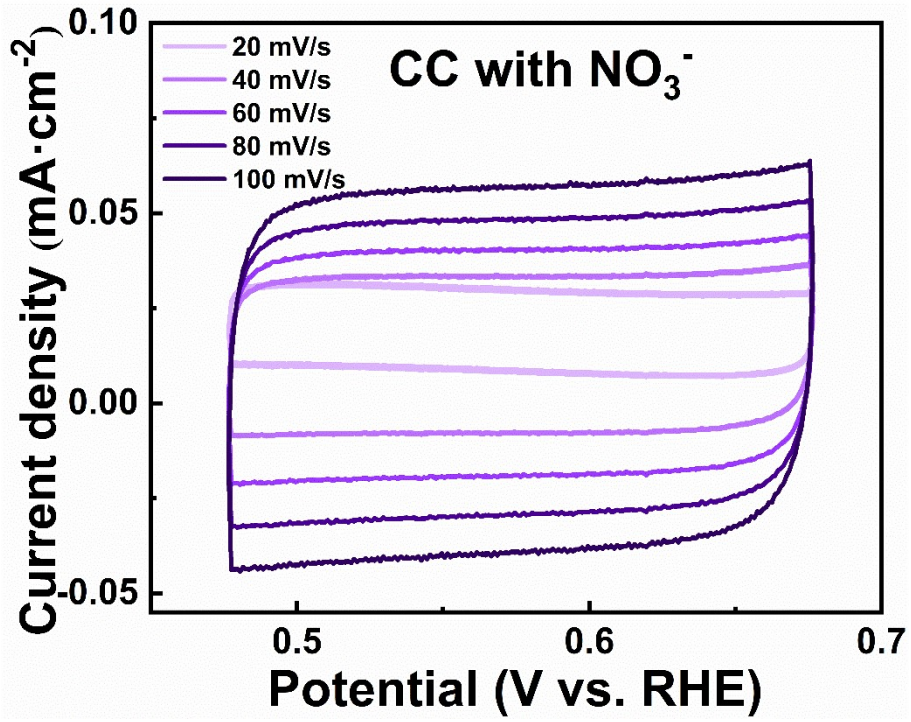

Fig. S9. The Plot of C for CC with nitrate in an argon environment.

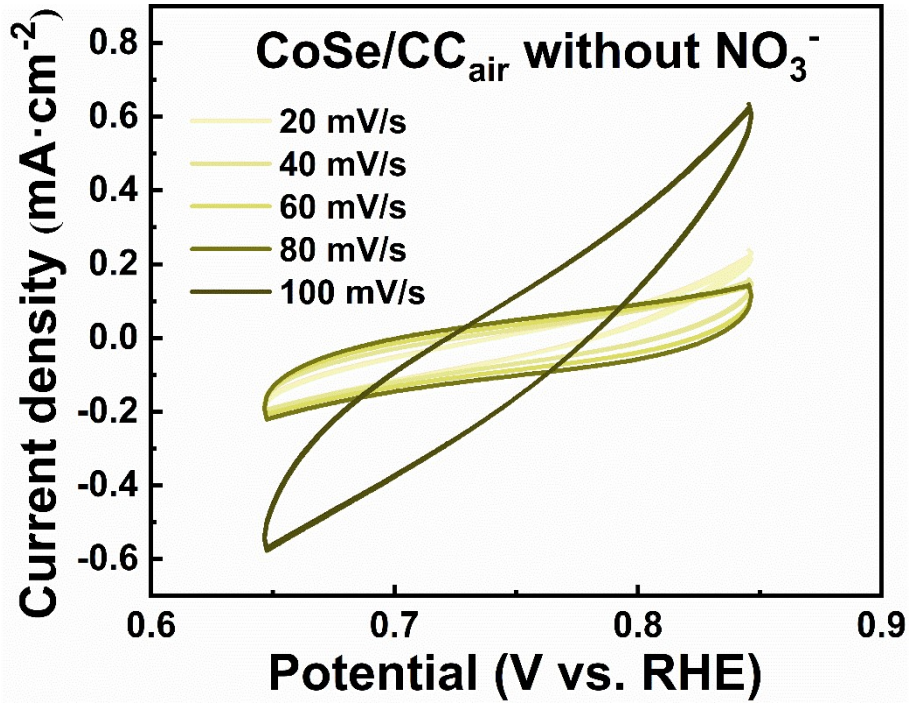

Fig. S10. The Plot of CV for CoSe/CC in the absence of nitrate in the air environment.

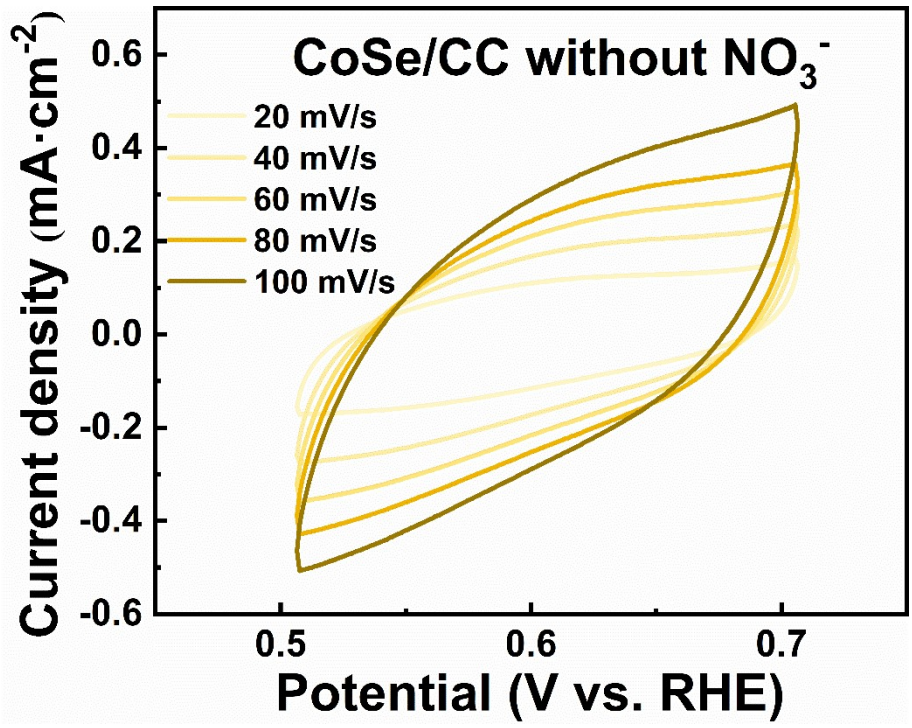

Fig. S11. The Plot of CV for CoSe/CC without nitrate in an argon environment.

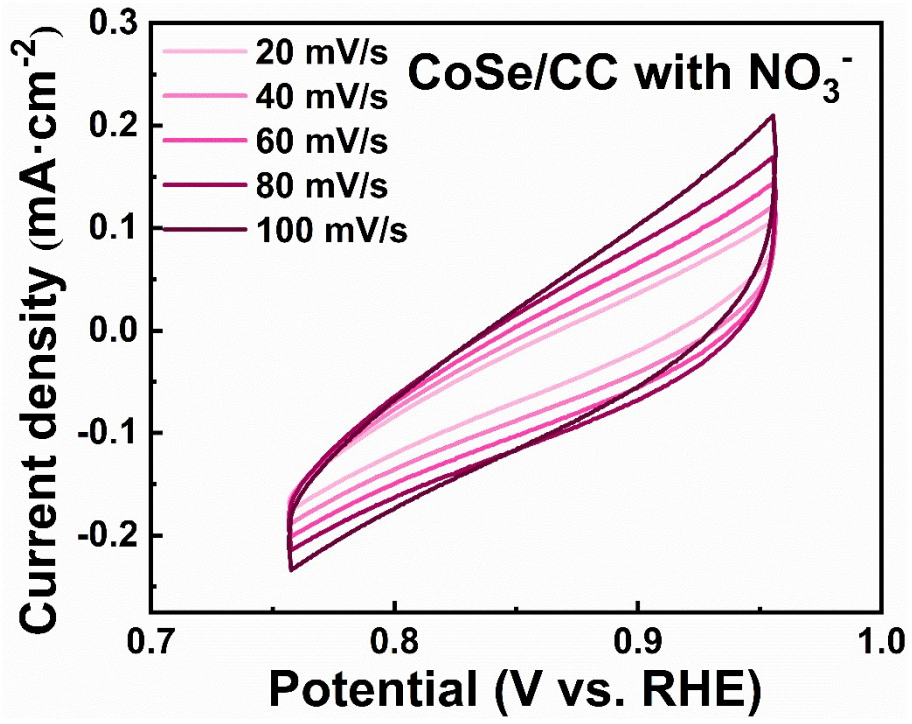

Fig. S12. The Plot of CV of CoSe/CC with nitrate in argon environment.

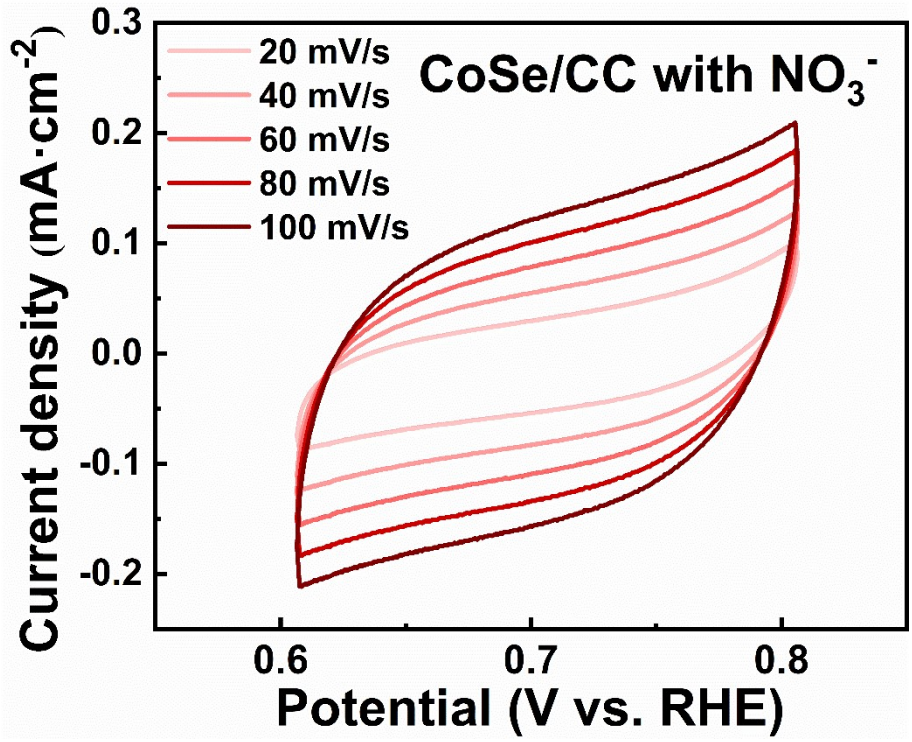

Fig. S13. The Plot of CV for CoSe/CC with nitrate in the air environment.

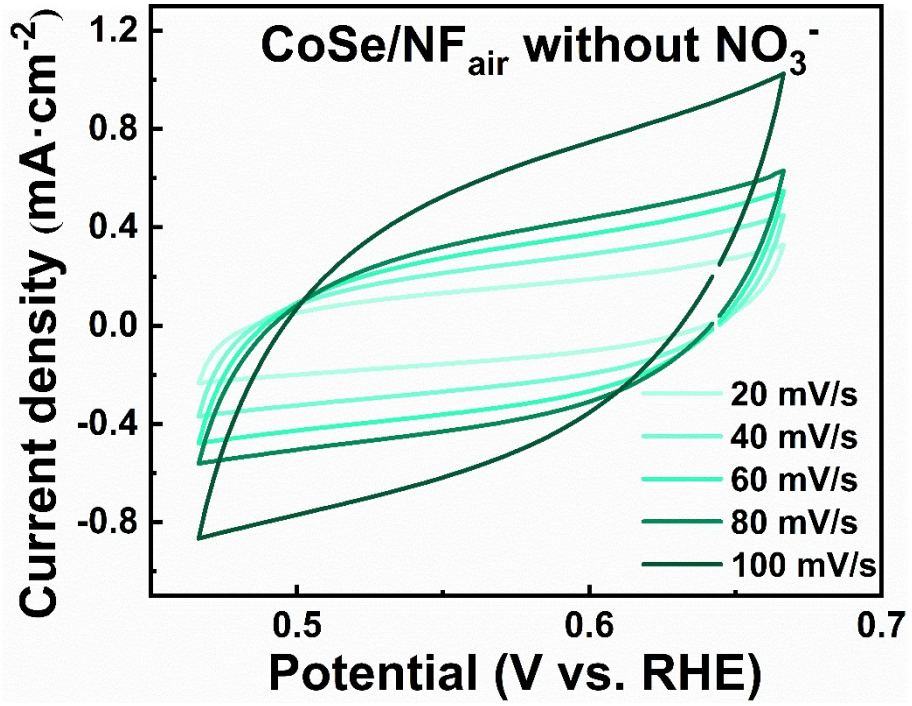

Fig. S14. The Plot of CV for CoSe/NF in the absence of nitrate in an air environment.

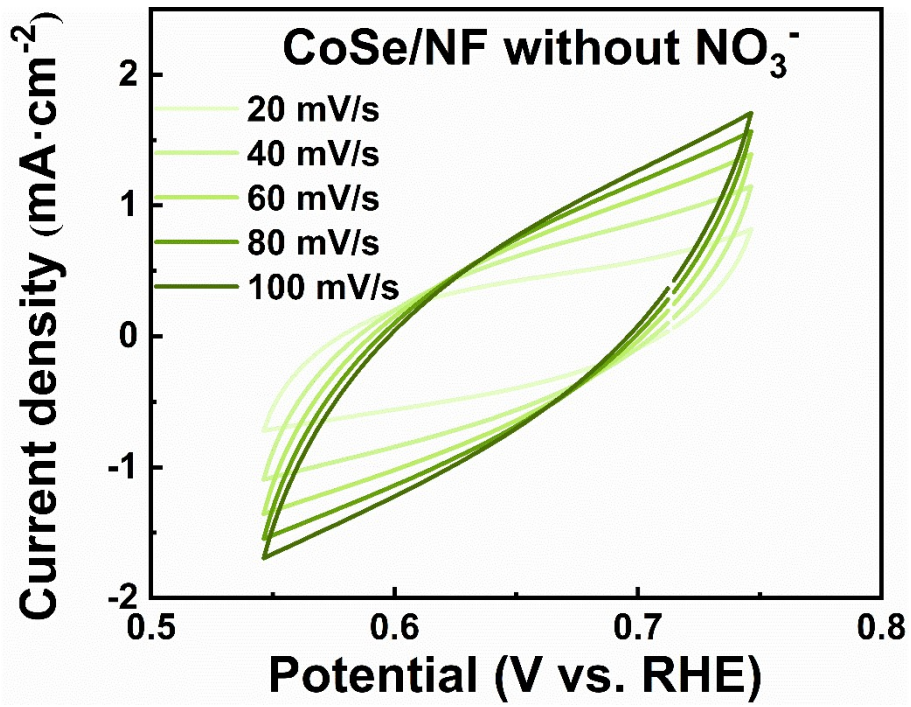

Fig. S15. The Plot of CV for CoSe/NF without nitrate in an argon environment.

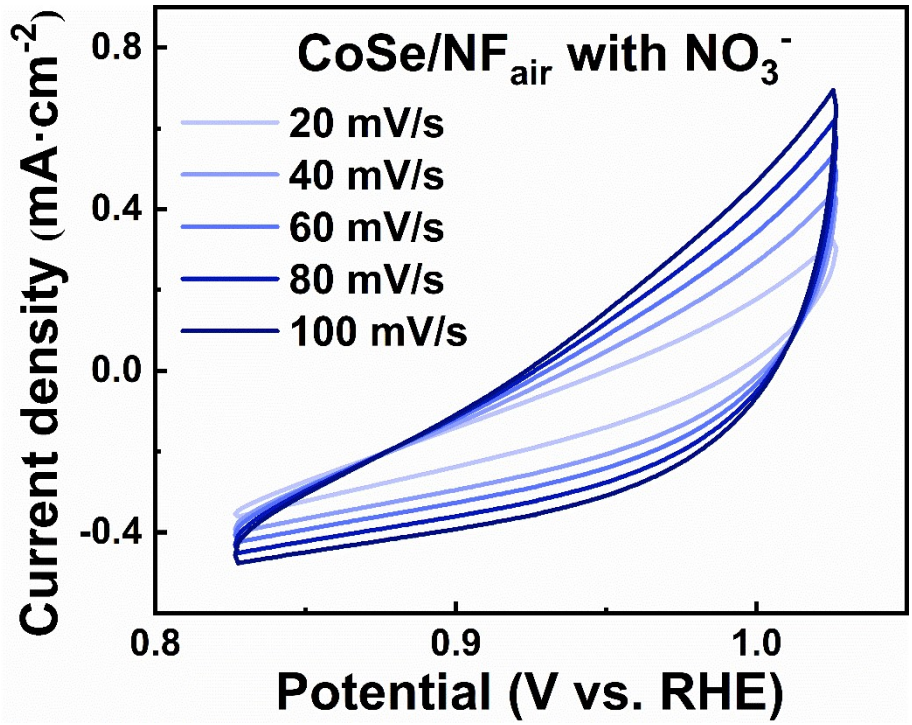

Fig. S16. The Plot of CV for CoSe/NF with nitrate in air environment.

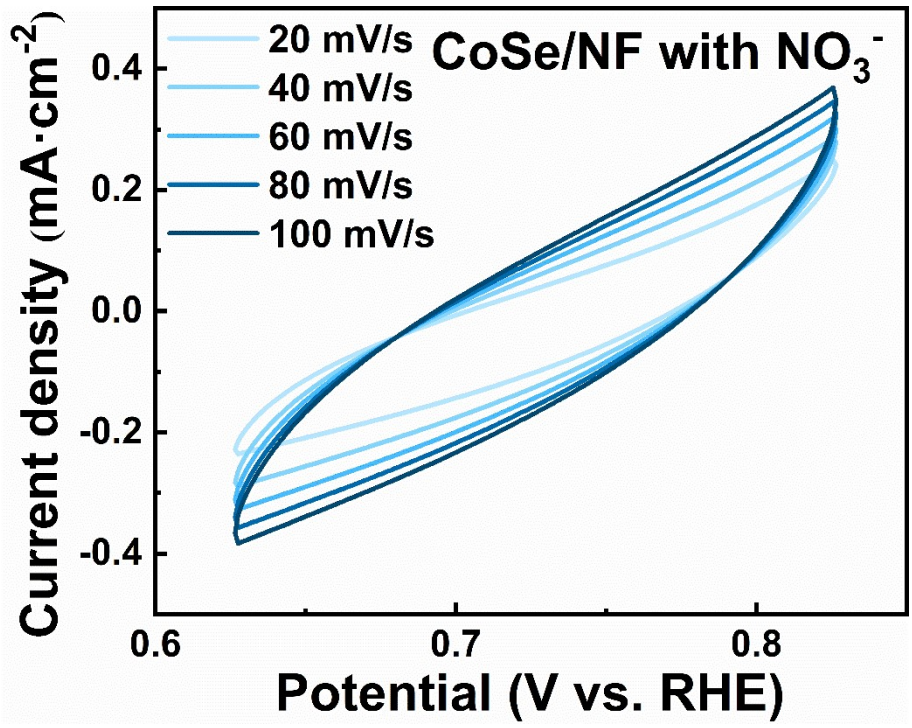

Fig. S17. The Plot of CV of CoSe/NF with nitrate in argon environment.

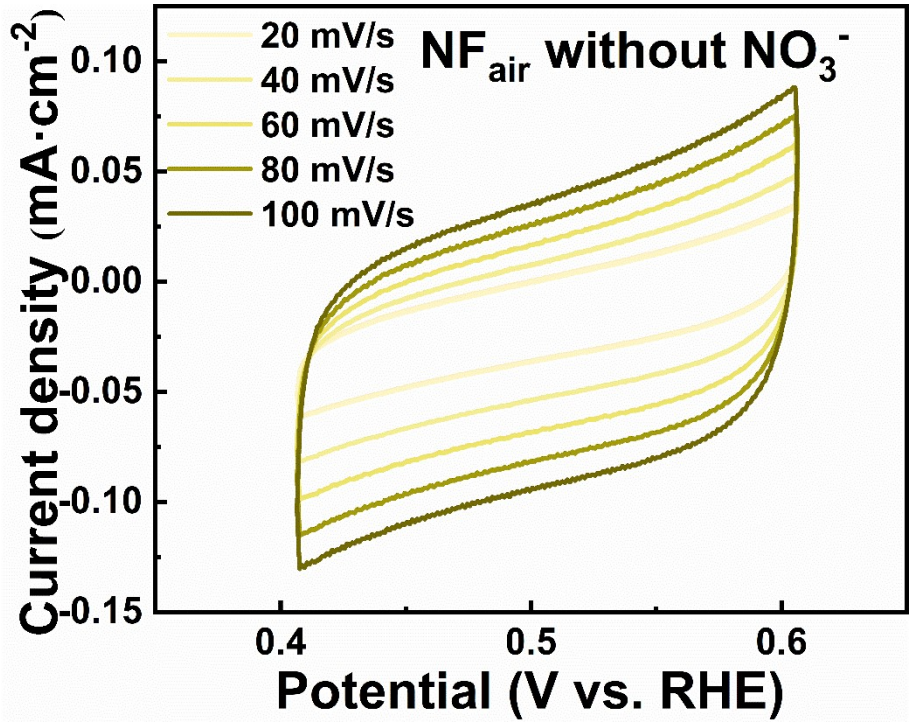

Fig. S18. The Plot of CV for NF in the absence of nitrate in the air environment.

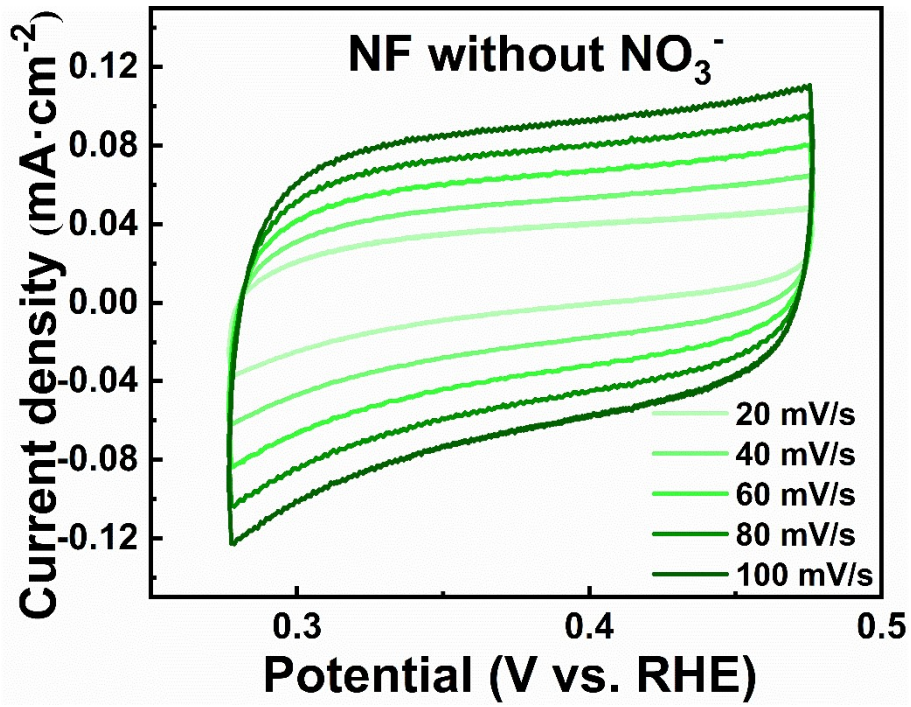

Fig. S19. The Plot of CV for NF in argon environment without nitrate.

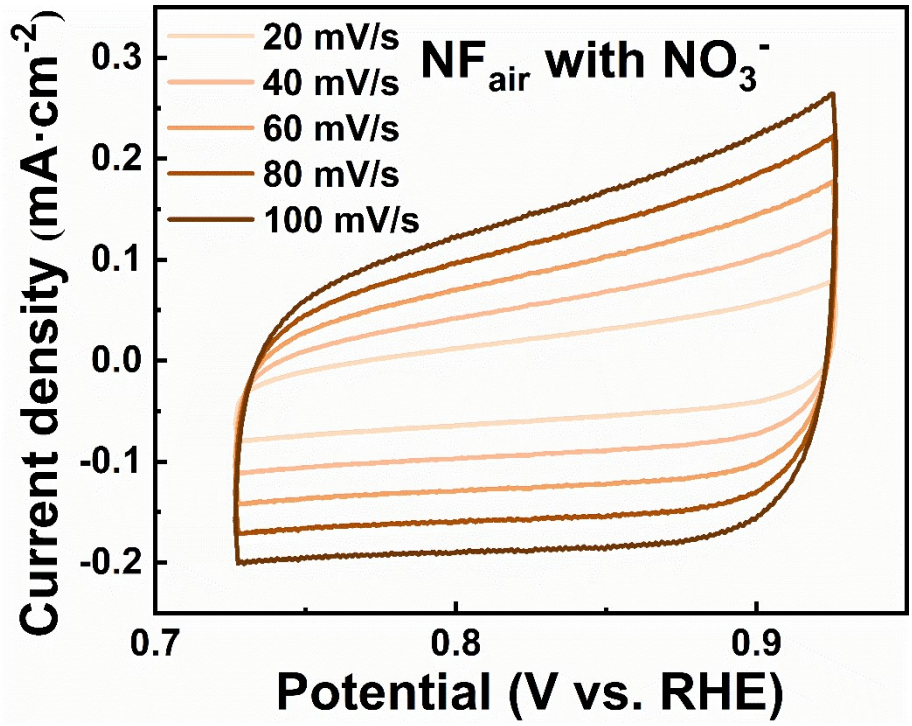

Fig. S20. The Plot of CV for NF with nitrate in the air environment.

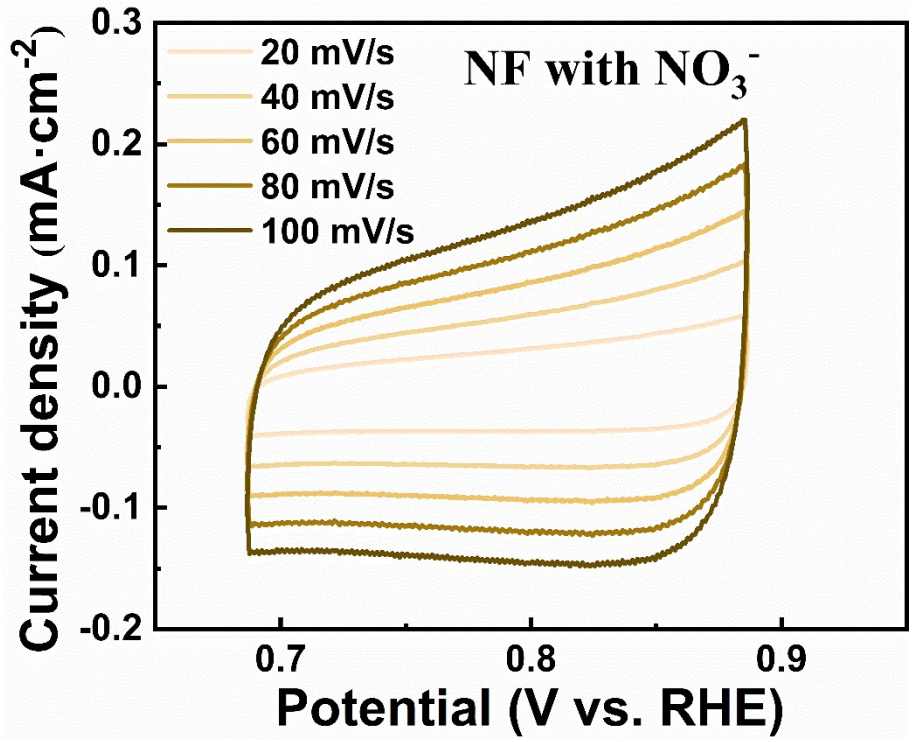

Fig. S21. The Plot of CV for NF with nitrate in an argon environment.

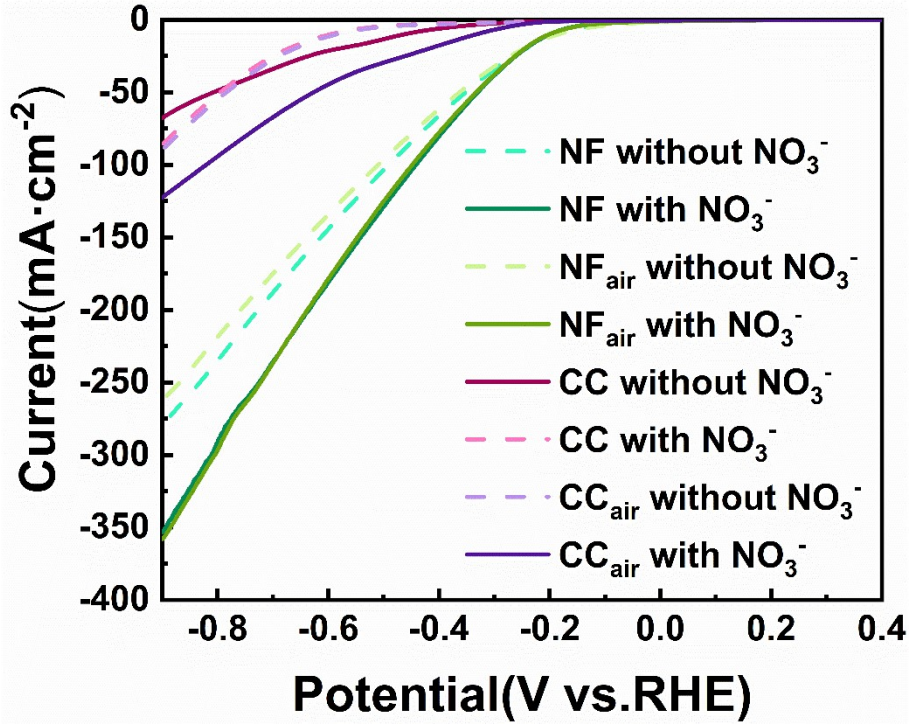

Fig. S22. LSV curve for NF and CC.

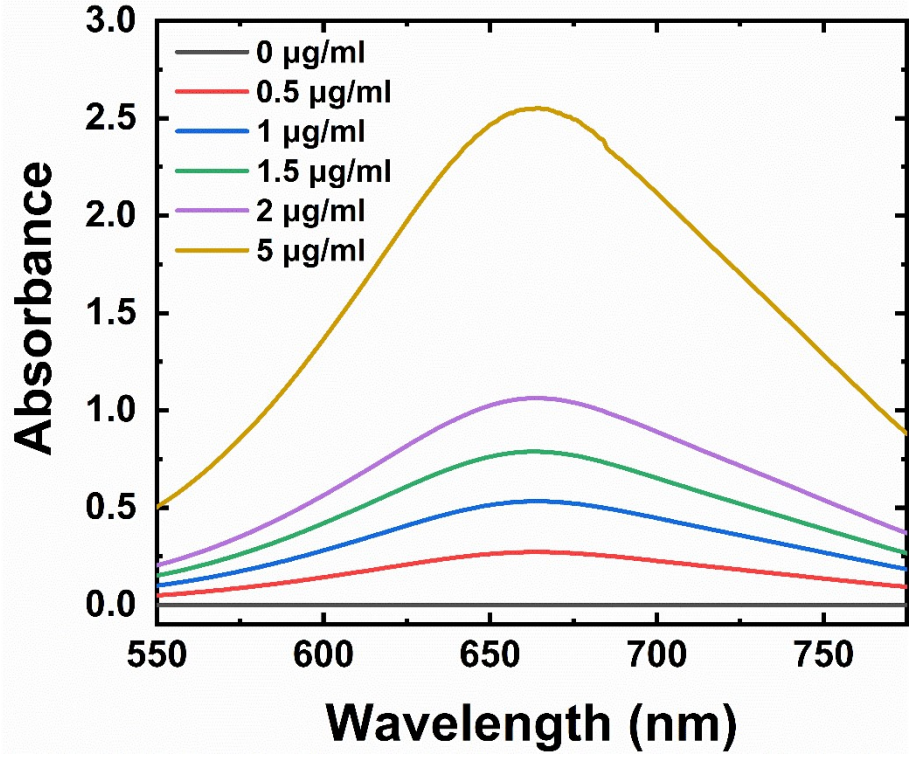

Fig. S23. UV absorption spectrum of NH_3.

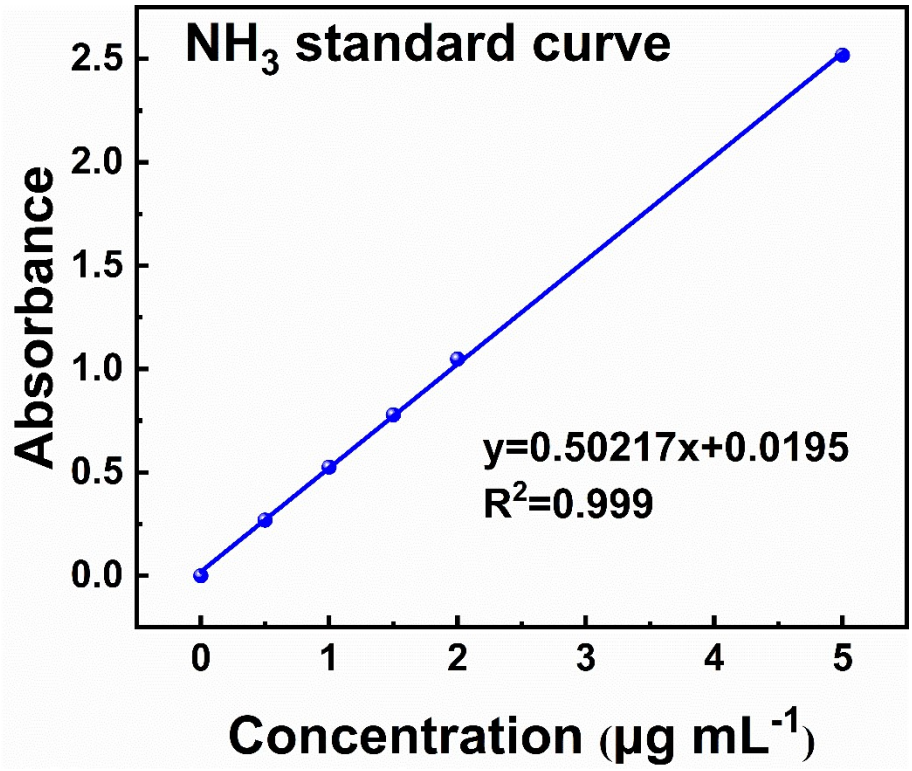

Fig. S24. Standard curve for NH_3.

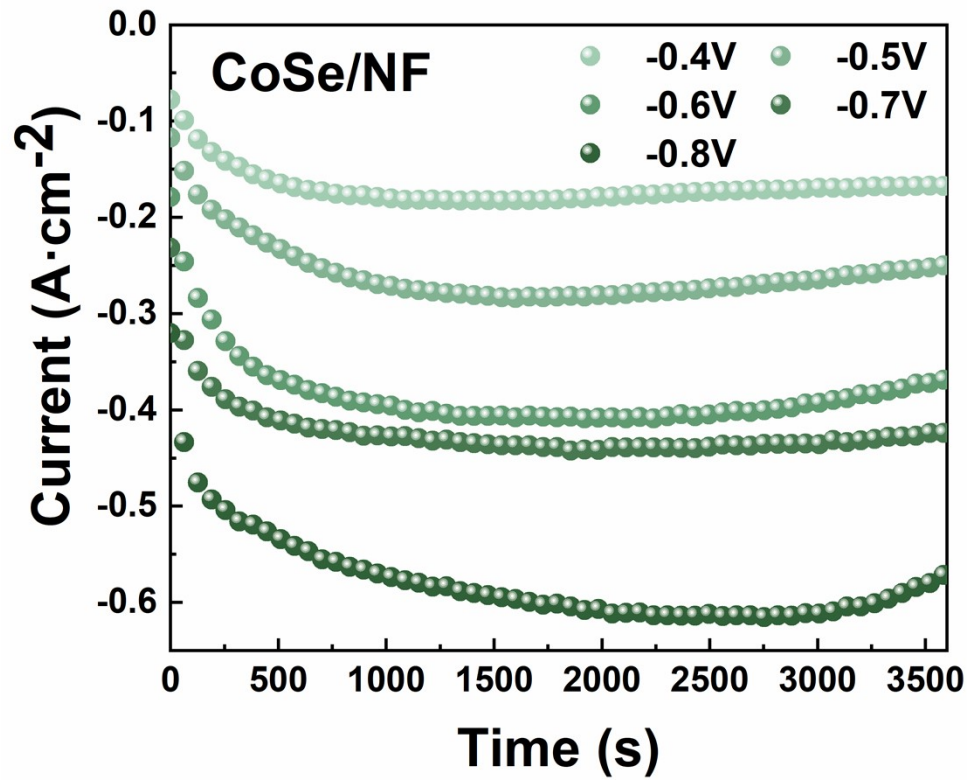

Fig. S25. Chronoamperometry measurements curve for CoSe/NF.

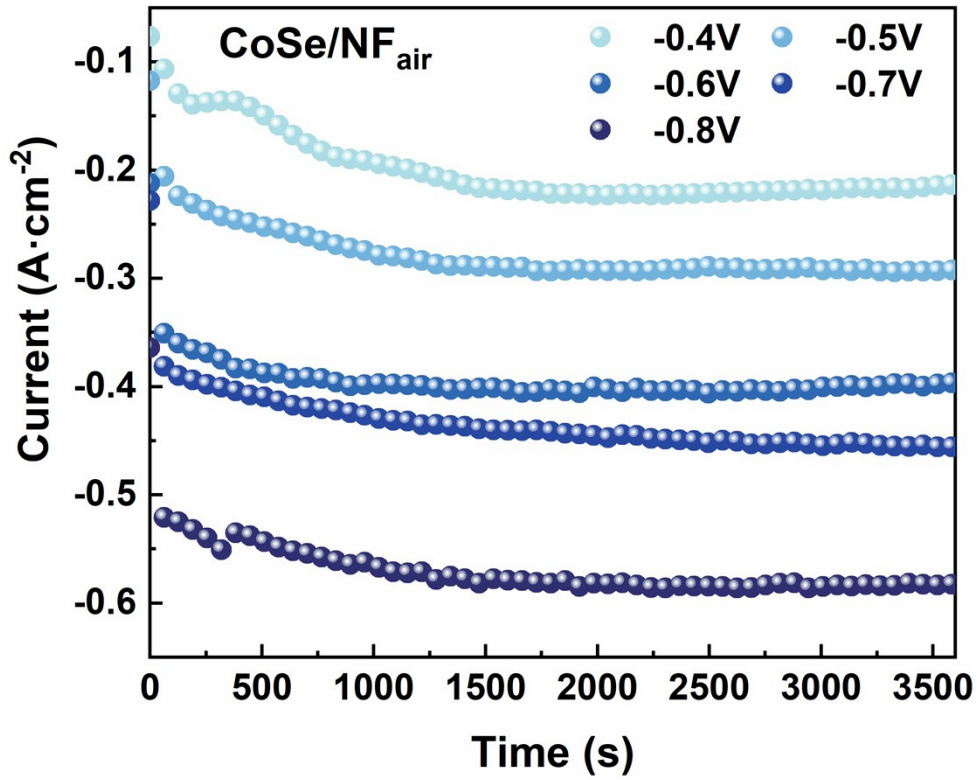

Fig. S26. Chronoamperometry measurements curve for $CoSe/NF_{air}$.

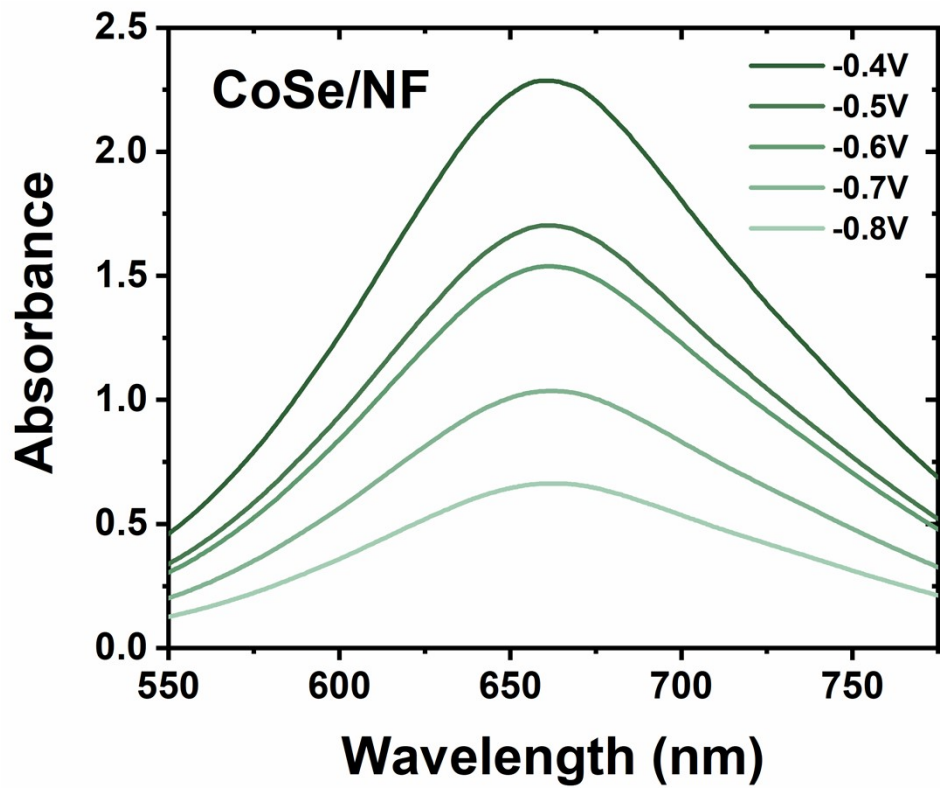

Fig. S27. UV absorption spectrum of CoSe/NF.

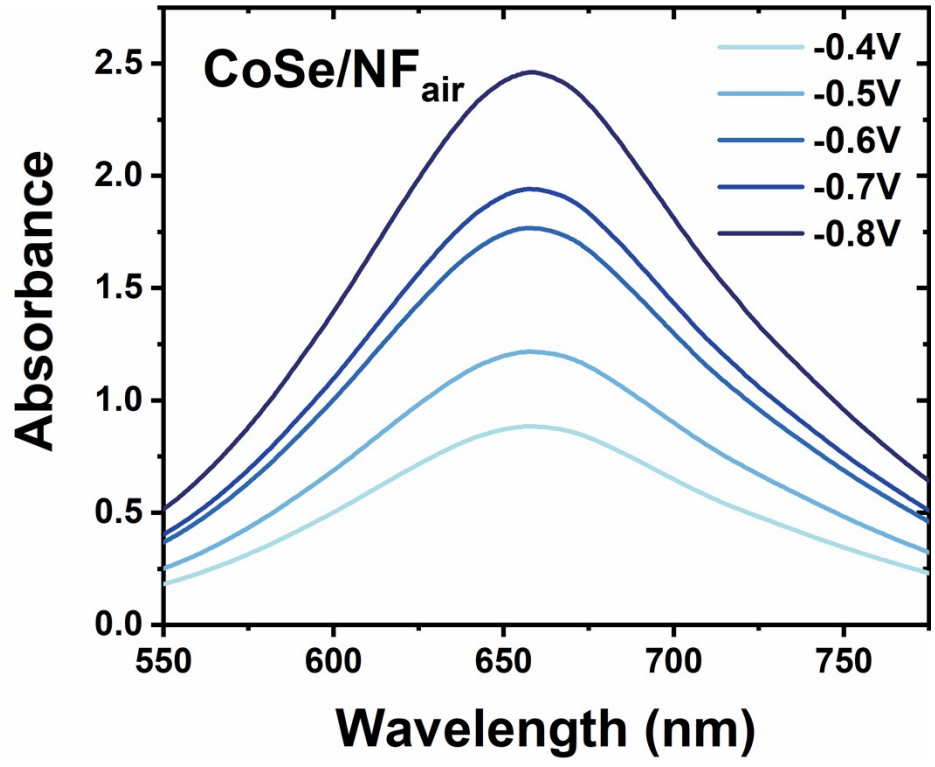

Fig. S28. UV absorption spectrum of $CoSe/NF_{air}$.

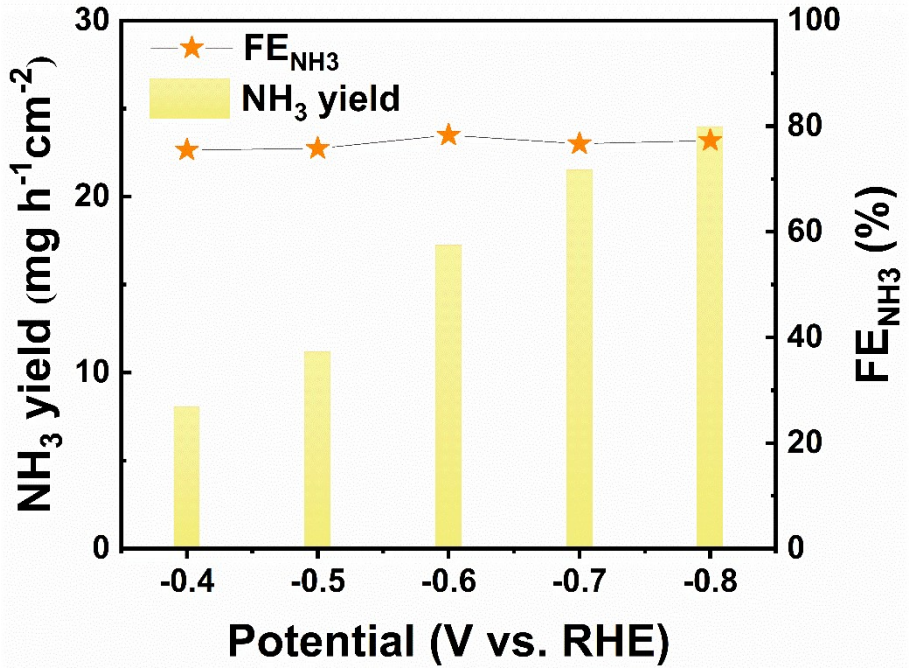

Fig. S29. Performance plot of CoSe/NF tested in an argon environment after activation in an air environment.

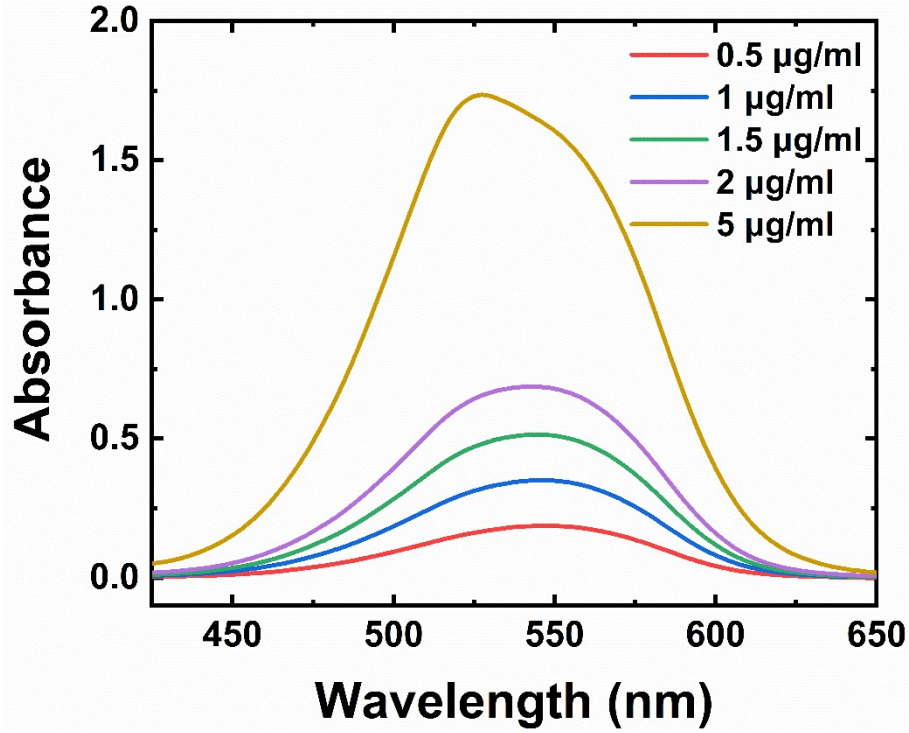

Fig. S30. UV absorption spectrum of NO_2.

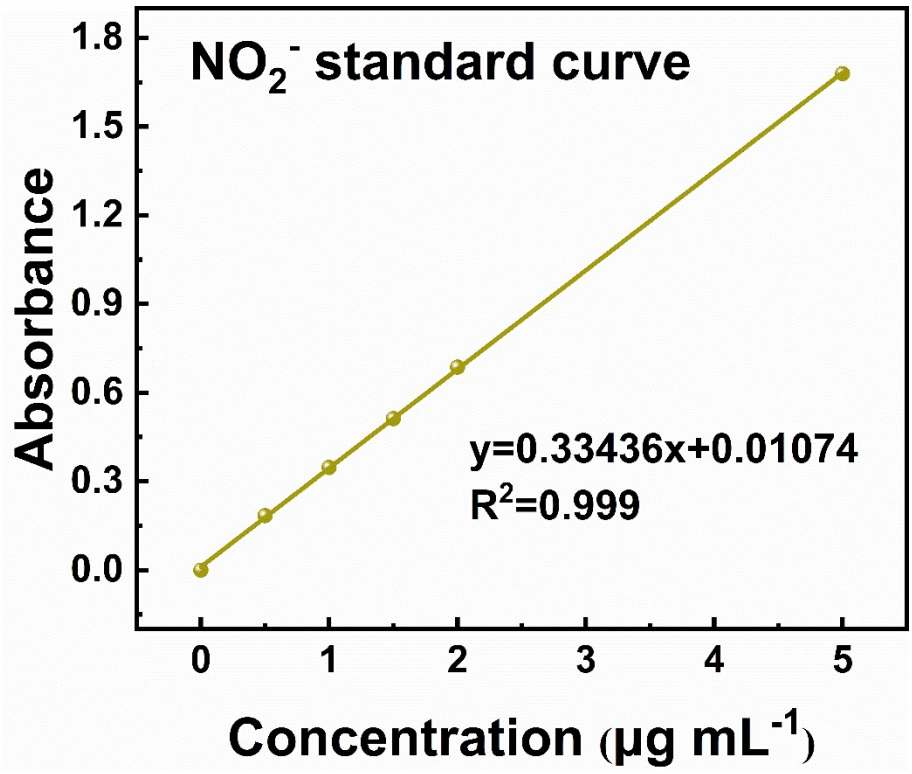

Fig. S31. Standard curve for NO_2.

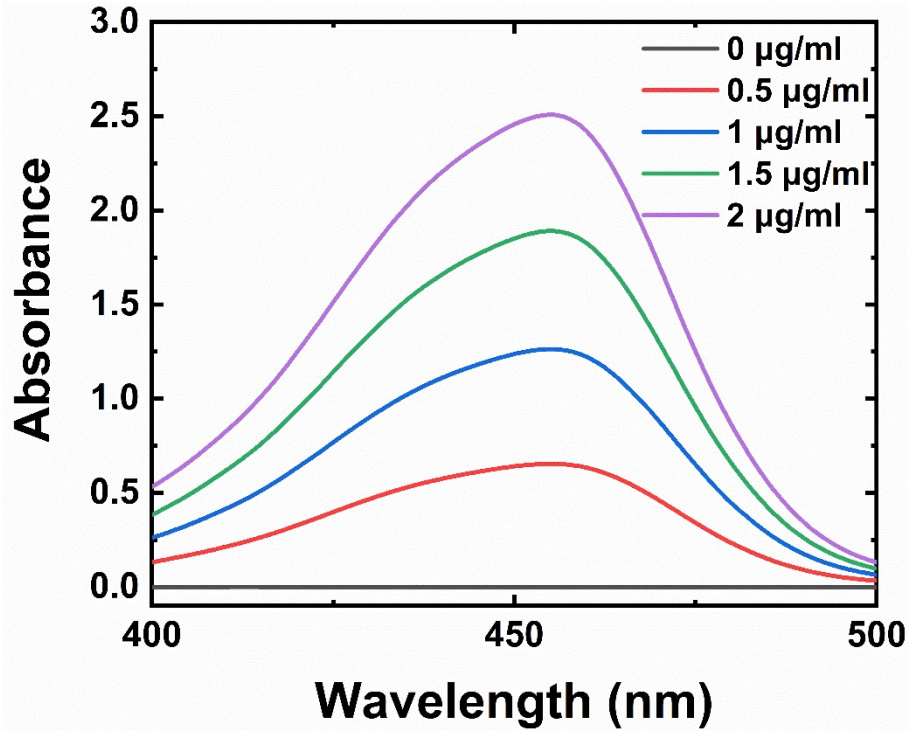

Fig. S32. UV absorption spectrum of N_2H_4.

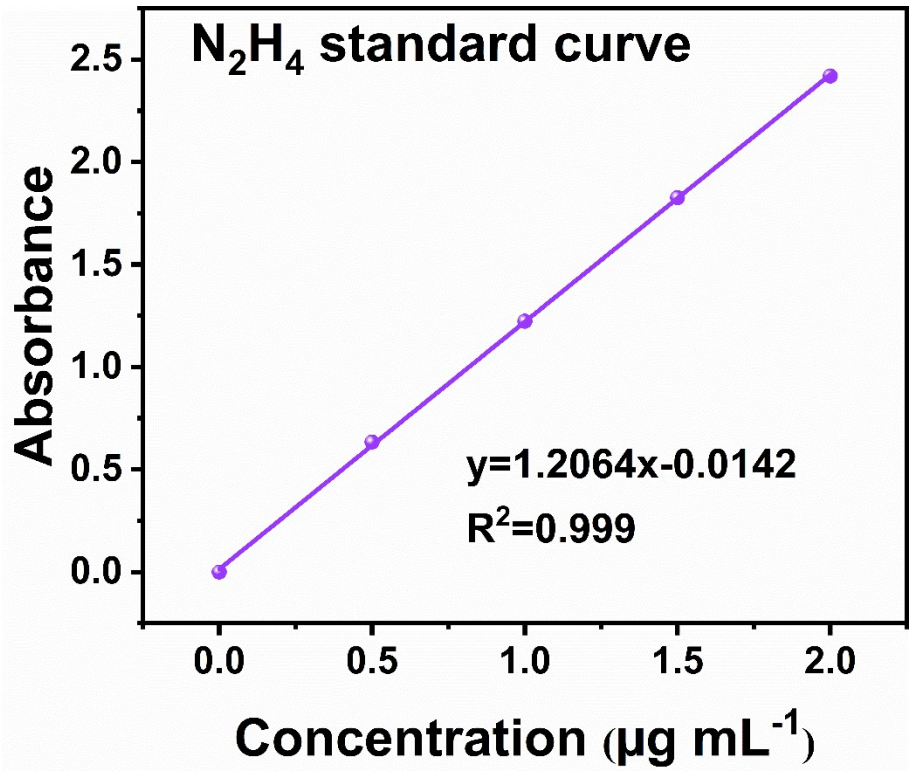

Fig. S33. Standard curve for N_2H_4.

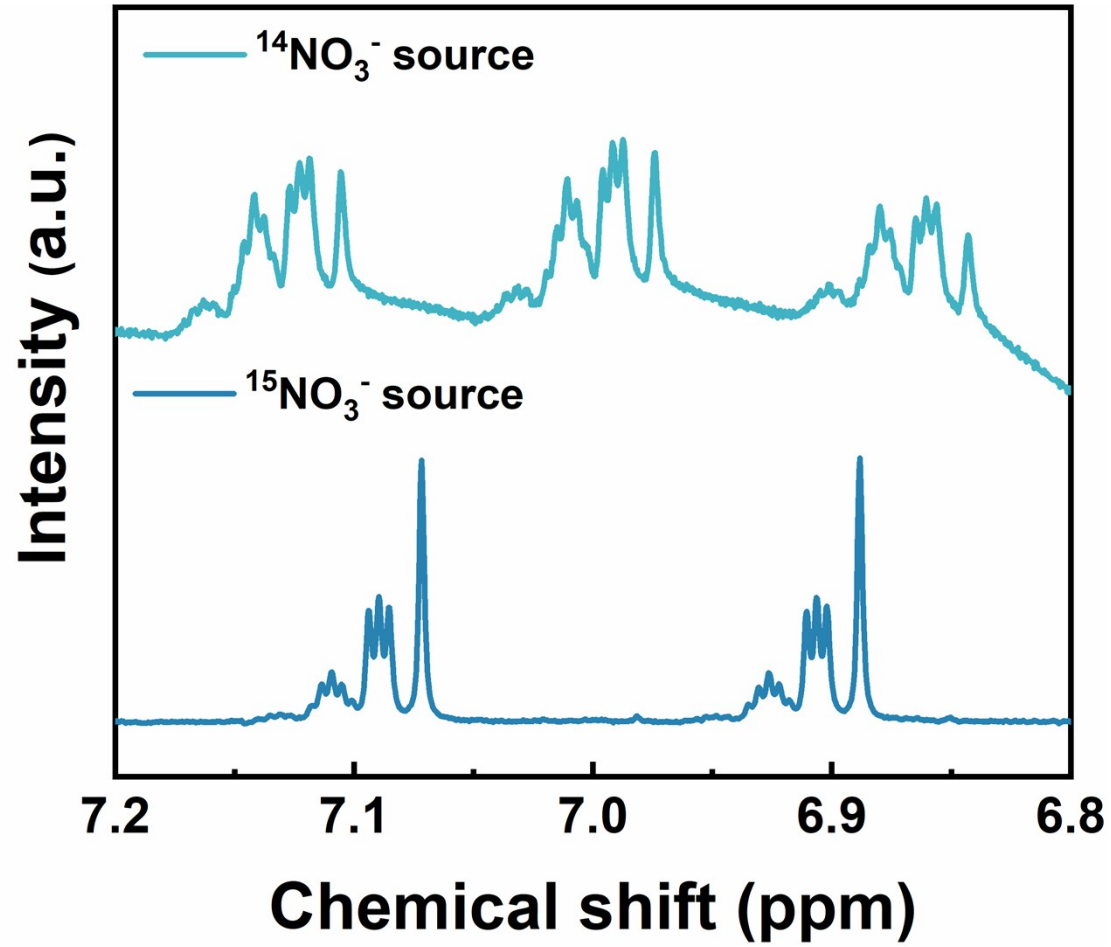

Fig. S34. ^1H NMR measurement after NO_3RR electrolysis

[1] S. Hoekx, N. Daems, D. Arenas Esteban, S. Bals, T. Breugelmans. Toward the Rational Design of Cu Electrocatalysts for Improved Performance of the NO3RR, ACS Appl. Energy Mater. 2024 7 3761–3775.

[2] Y. Sun, Y. Shi, Y. Gao, M. Sun, Y. Yao, H. Yu, Y. Xu, X. Wang, Y. Yang. Electroreduction of nitrate into ammonia on Co3O4: Mechanistic insights into Co2+-promoted NO3RR performance, Chem. Eng. J. 2025 512 162506.

[3] J. Yue, S. Liping, W. Yuechen, H. Lihua, Z. Hui. Enhanced electrocatalytic nitrate reduction and energy conversion through Zn–Nitrate battery by Cu3P@Co(OH)2/CF heterostructure catalyst, Int. J. Hydrogen Energy 2024 71 820–830.

[4] X. Wang, J. Ren, Z. Gao. Self–supported copper–cobalt oxide hybrid electrode for bifunctionally electrocatalytic nitrate reduction and methanol oxidation reactions, J. Colloid Interface Sci. 2025 693 137575.

[5] H. Zhou, Y. Kong, M. Zuo, Y. Chen, Y. Sun, S. Li, L. Han. Enhancement of Nitrate–to–Ammonia Over La(OH)3@CuCo Alloy Heterostructures via the Integration of Interface Engineering and Co Alloying, Small 2025 21 2502527.

[6] W. Tao, P. Wang, H. Li, R. Huang, G. Zhou. Engineering sulfur vacancies optimization in Ni3Co6S8 nanospheres toward extraordinarily efficient nitrate electroreduction to ammonia, Appl. Catal., B 2023 324 122193.

[7] W. Qiu, Y. Guo, X.–Z. Fu, J.–L. Luo. Prussian Blue Derived High–Entropy Alloy Catalysts for Enhanced Electrochemical Nitrate Reduction to Ammonia, Adv. Funct. Mater. 2025 35 2415970.

[8] Z. Gu, Y. Zhang, X. Wei, Z. Duan, Q. Gong, K. Luo. Intermediates Regulation via

Electron–Deficient Cu Sites for Selective Nitrate–to–Ammonia Electroreduction, Adv. Mater. 2023 35 2303107.

[9] I. Kuznetsova, D. Kultin, O. Lebedeva, S. Nesterenko, E. Murashova, L. Kustov, Intermetallic Compound and Solid Solutions of Co75Me25 (Me: Si, Fe, Cr) as Catalysts for the Electrochemical Reaction of Nitrate Conversion to Ammonia, in: International Journal of Molecular Sciences, 2025, pp. 1650.